Electron correlations in the two-dimensional Hubbard model: A group-theoretical and numerical study

G. Fano and F. Ortolani
Dipartimento di Fisica, Università di Bologna, via Irnerio 46, I-40126 Bologna, Italy

A. Parola
Dipartimento di Fisica, Università di Milano, via Celoria 16, I-20133 Milano, Italy
(Received 6 August 1991)

The Lanczos algorithm has been applied to the Hubbard model on a 4×4 square lattice and several equal-time correlation functions have been evaluated. This computation has been made possible by a classification of all the irreducible representations of the space symmetry group, which allowed a considerable reduction of the dimension of the Hilbert space of the system. Such an analysis is quite general and might be useful in other physical applications. Our results shed light on the effects of doping on the magnetic ordering, suggest a spin-charge decoupling at large U, and show a remarkable reduction of the quasiparticle weight at strong coupling.

I. INTRODUCTION

The renewed interest in simple models of interacting electrons, stimulated by the discovery of high-temperature superconductivity, has shown the weakness of the usual theoretical treatments of these systems and the lack of general consensus on their physical properties.[1] The apparent simplicity of the starting Hamiltonians, characterized by just a hopping term and a short-range interaction, hides the intrinsic complexity of these models which can generate strong electron correlations and several distinct phases by varying the external physical parameters. In fact, even the physical properties of the simplest model of interacting electrons, the Hubbard model, are not a settled issue yet.

The Hubbard Hamiltonian

$$H=-t\sum_{\langle i,j\rangle,\sigma}c^{\dagger}_{j,\sigma}c_{i,\sigma}+U\sum_{i}n_{i,\uparrow}n_{i,\downarrow} \tag{1.1}$$

describes electrons on a square lattice with nearest-neighbor hopping ($t=1$) and on site repulsion ($U>0$). At half filling (i.e., for electron density $\rho=1$), it is the prototype of Mott insulators, characterized by antiferromagnetic long-range order,[2] but when holes are injected into the system, it might show quite different behaviors. In particular, it has been argued to undergo superconductivity[3] or phase separation[4] at strong coupling, and to violate Fermi-liquid theory in the whole phase diagram in any dimension.[5]

The theoretical approaches that have been applied to the investigation of the Hubbard model make use of all available techniques in many-body physics. Standard Hartree-Fock calculations, based on a "magnetic" decoupling of the interaction term,[6] give rise to a phase diagram characterized by an insulating state at half filling and metallic behavior at finite doping. The presence of a Mott transition at half filling (and $U=0^{+}$) is a consequence of the nesting property of the Fermi surface which induces diverging antiferromagnetic fluctuations within perturbation theory. This conclusion agrees with weak-coupling diagrammatic approaches based on spin-density wave theory[7] or random-phase approximation.[8] These studies also suggest the existence of effective hole-hole attraction at low doping mediated by local antiferromagnetic order which, in turn, might provide a microscopic mechanism for superconductivity. Also more refined self-consistent diagrammatic resummations are being attempted in the doped regime and preliminary results compare favorably with weak-coupling simulation data.[9] The low-density (i.e., heavy doped) regime has been recently investigated in order to understand the possible breakdown of perturbation methods or of Fermi-liquid theory in these systems.[10]

The Hubbard model has been also directly attacked by the strong-coupling side, the so called t-J model, mainly in the physically relevant low-doping regime. Here ordinary perturbation theory is not available anymore because of the restriction of single occupancy of each site, which makes the "noninteracting" ($J=0$) problem already a formidable task. However, perturbation methods can still be used, provided that the model is suitably generalized by considering spin-S particles instead of electrons and taking the large-S limit. In such a framework, both self-consistent diagrammatic methods[11] and semiclassical approaches[12] have been applied to the study of the dynamical properties of a single hole. These analyses suggest that, except in one dimension, the Hubbard model belongs to the class of Fermi liquids, as far as the charge properties are concerned, while unconventional antiferromagnetic order might be induced by doping. In fact, the effect of doping on the magnetic structure of the system is still a controversial issue and several possibilities have been proposed: ferromagnetic polarons,[13] domain walls,[14] spiral long-range order,[12] or even more exotic arrangements.[15]

Similarly, slave-bosons[16] (or Schwinger boson[17]) ap-

proaches are systematic methods for calculating the phase diagram of models at strong coupling by employing perturbation theory in an *ad hoc* parameter which, physically, governs the introduction of quantum fluctuations in the system. This method gives good results in pure (undoped) antiferromagnets where the spin-wave spectrum is accurately reproduced but, in doped systems, suffers from a certain degree of arbitrariness in the choice of the expansion parameter. Slave bosons have been recently shown to agree quantitatively with simulation data in the Hubbard model at weak coupling.[18] Finally, more refined mean-field theories,[19] with unconventional decoupling of the interaction term, give rise to very rich phase diagrams, characterized by exotic phases (like dimer, chiral, and flux phases) leading to the breakdown of Fermi-liquid theory and to fractional statistic of the elementary excitations.[20]

Each of these methods probably capture parts of the physics of strongly correlated electron systems, and often it is difficult to test the differences between predictions of different theories. All methods basically agree on the short-range behavior of the correlation functions, such as the presence of local antiferromagnetic order at low doping, or the k_F oscillations of the one-particle density matrix. The crucial differences are instead contained in subtle long-wavelength properties, such as the presence of true long-range order or the smoothing of the jump in the momentum distribution or the statistic of quasiparticles. Similar problems have been already encountered in one-dimensional models where a very accurate finite-size scaling is required in order to distinguish between Fermi-liquid and Luttinger-liquid behavior.[21] This circumstance partly explains the apparent agreement of different theories with simulations in the Hubbard model. Unfortunately, an accurate description requires a considerable numerical effort and, often, simulation data are not precise enough for this purpose. That is the reason why only a careful comparison between the theoretical predictions and the "exact" numerical solution of the model in finite systems can test the validity of the different scenarios which have been proposed.

This program has been already undertaken for the t-J model where the Lanczos algorithm has been successfully applied in square lattices with up to 20 sites.[22] The evaluation of ground-state energies for few holes, supported by the hole-hole correlation function, has shown the tendency of holes to bind for J larger than a critical limiting value J_c ($J_c \sim 0.1$ in the lattices considered). However, no clear-cut argument has been given for the actual occurrence of superconductivity in the model, while phase separation seems the likely outcome. The absence of simulation results for larger lattices prevents a clear extrapolation of these results to the thermodynamic limit and the issue of phase separation in the model is still controversial. Dynamical properties, such as optical conductivity and the one-hole Green's function, have also been evaluated by the Lanczos technique in the t-J model[23,24] and evidence for a quasiparticle peak has been reported in several investigations. Here the problem of interpretation is even more difficult than for static quantities. In fact the thermodynamic limit of dynamical quantities requires a coarse graining along the frequency axes, which washes out many features present in finite systems. This is particularly evident in the numerical computation of the one-hole Green's function in one dimension where exact results are now available.[25] Notwithstanding the accuracy of the computations and the better k-space resolution that can be obtained in one dimension, the numerical data in 16-site rings[24] failed to show a clear evidence of the branch cut singularity, which is now believed to occur in the spectral weight, and only the bandwidth can be safely deduced from these studies.

In order to get more information about the properties of strongly correlated electron systems in two dimensions, it is useful to investigate the properties of the Hubbard model in small clusters by the Lanczos technique. We believe that the Hubbard model has two important advantages with respect to the t-J model:

(i) The existence of an interaction parameter (U) allows one to follow the growth of correlations from $U=0$ to strong coupling. Therefore, correlation effects are more clearly singled out, contributing to the physical understanding of the model.

(ii) The existence of Monte Carlo simulation for the Hubbard model at weak or intermediate coupling,[2,26] also gives some help in the interpretation of the results. In particular, if some general feature is seen to persist also in the larger system, finite-size effects can be easily ruled out and the physically relevant information can be safely extracted from diagonalization data.

Unfortunately, the Hilbert space of the Hubbard Hamiltonian is much larger than that of the t-J model, and this circumstance has heavily limited the application of the Lanczos technique to this model. In particular, the interesting case of a 4×4 lattice has been previously investigated[27] only at $U=4$ and an extensive survey of the results for different values of the interaction is still missing. In this paper, we show how it is possible, by exploiting the spatial symmetries of the lattice, to reduce the dimension of the Hilbert space of the Hubbard model on a 4×4 lattice by two orders of magnitude. The group-theoretical framework (which is completely general and can be applied also to other many-electron systems with a large space group of symmetry) is described in Sec. II; (a preliminary account of the method was given in Ref. 28). The particular space group of the Hubbard model on a rectangular lattice is analyzed in the Appendix, where all the irreducible representations are classified and written down in an explicit way. These irreducible representations are labeled by five quantum numbers, i.e., the usual momenta k_x and k_y, and three indexes related to the parity under the reflections $x'=-x$, $y'=-y$, and $x'=y$, $y'=x$. This abstract approach allows an efficient implementation of the Lanczos algorithm on a supercomputer. Of course, the symmetries of the problem are not exhausted by the space group. There are two important symmetries left: the well-known spin SU(2) symmetry, and the very interesting, recently discovered[29] SU(2) pseudospin symmetry. However, the implementation of the Lanczos method by taking into account all possible quantum numbers is quite a demanding task.

The problem of the hole binding and the hole-hole

correlations studied in Ref. 30 were analyzed by the present method, as well as some recent numerical results on the density of states of 4×4 clusters.[31]

Here we apply this technique to the computation of several (equal-time) correlation functions in the Hubbard model on a 4×4 lattice. The behavior of the magnetic as well as charge correlations when the interaction is turned on is studied together with the change in spin arrangements around a hole, momentum distribution, and quasiparticle weight. These results, presented in Sec. III, also shed some light on the character of the elementary excitations both in the charge and in the spin channel.

II. GROUP THEORY AND THE HUBBARD HAMILTONIAN

Let G denote the space group of order N_G of a system of n_u spin-up electrons and n_d spin-down electrons. G commutes with the Hubbard Hamiltonian and will be studied in detail. We denote by $c^\dagger_{i\sigma}$ the creation operator of an electron on the site i and spin σ. A configuration will be denoted by

$$|\phi,\bar{\phi}\rangle = c^\dagger_{i_1\uparrow}c^\dagger_{i_2\uparrow}\cdots c^\dagger_{i_{n_u}}c^\dagger_{j_1\downarrow}c^\dagger_{j_2\downarrow}\cdots c^\dagger_{j_{n_d}\downarrow}|0\rangle \ , \tag{2.1}$$

where ϕ denotes the set $\{i_1,i_2,\ldots,i_{n_u}\}$ and $\bar{\phi}$ the set $\{j_1,j_2,\ldots,j_{n_d}\}$. By definition of space group, the action of an element $g\in G$ can be specified as follows:

$$g|\phi,\bar{\phi}\rangle = |g\phi,g\bar{\phi}\rangle = c^\dagger_{gi_1\uparrow}c^\dagger_{gi_2\uparrow}\cdots c^\dagger_{gi_{n_u}\uparrow}c^\dagger_{gj_1\downarrow}c^\dagger_{gj_2\downarrow}\cdots c^\dagger_{gj_{n_d}\downarrow}|0\rangle \ . \tag{2.2}$$

Clearly the numbers n_u and n_d remain invariant under the action of g.

We denote by $R(G)$ the group ring. An element $x\in R(G)$ is a formal linear combination of elements of G: $x=\sum_g x(g)g$. The conjugate element x^+ is defined by $x^+=\sum_g \overline{x(g^{-1})}g$. (Representing the group elements g by unitary operators, x^+ becomes the Hermitian conjugate of x).

Let us write some known formulas that will be of help in the decomposition of the space of configurations in invariant subspaces. We denote by $\{D^j(g)\}$ a unitary irreducible representation of G of dimension d_j. The standard basis in $R(G)$ is defined by

$$v^j_{\mu m}=\sqrt{d_j/N_G}\sum_g D^j_{\mu m}(g^{-1})g \ . \tag{2.3}$$

These vectors obey the relations, for any $\tilde{g}\in G$,

$$\tilde{g}v^j_{\mu m}=\sum_n D^{(j)}_{nm}(\tilde{g})v^j_{\mu n} \ , \tag{2.4}$$

$$v^j_{\mu m}\tilde{g}=\sum_\nu D^j_{\mu\nu}(\tilde{g})v^j_{\nu m} \ , \tag{2.5}$$

$$\tilde{g}=\sqrt{d_j/N_G}\sum_{j,\mu,m} D^j_{m\mu}(\tilde{g})v^j_{\mu m} \ , \tag{2.6}$$

$$v^{j\dagger}_{\mu m}=v^j_{m\mu}, \quad v^{j\dagger}_{mm}=v^j_{mm} \ , \tag{2.7}$$

$$v^{j'\dagger}_{\mu' m'}v^j_{\mu m}=\sqrt{N_G/d_j}\,\delta_{jj'}\delta_{mm'}v^j_{\mu\mu'} \ . \tag{2.8}$$

The operators

$$P^j_m=\sqrt{d_j/N_G}\,v^j_{mm} \tag{2.9}$$

become projection operators on the invariant subspaces when we represent the group by unitary operators [see, e.g., Eq. (2.2)]. They obey the relations [where e denotes the identity of $R(G)$]

$$\sum_{j,m}P^j_m=e \ , \tag{2.10}$$

$$P^{j'}_{m'}P^j_m=\delta_{jj'}\delta_{mm'}P^j_m \ . \tag{2.11}$$

Let us now consider the configurations of a definite type of spin (up or down); we shall say that the configurations a and b are *equivalent* if $\exists g\in G$ such that

$$ga=\pm b=(-1)^{S(g,a)}b \ . \tag{2.12}$$

For instance, b can be obtained from a by a translation. The configurations a and b have the same aspect, except the cases when, due to the periodic boundary conditions, part of the configuration a is shifted by g on the opposite side of the lattice (see Fig. 1). The phase factor ±1 is due to Fermi statistics. The equivalence relation $a\sim b$ allows one to partition the configurations of definite spin (up or down) into equivalence classes.

We denote by O_a the *orbit* generated by the configuration a, i.e., the set

$$O_a=\{ga,\ g\in G\} \ . \tag{2.13}$$

The number N_a of distinct configurations belonging to the orbit O_a is in general less than N_G; indeed it is possible that $g_1a=\pm g_2a$, i.e., $g_2^{-1}g_1a=\pm a$. If the configuration a is highly symmetrical, the orbit is small. For instance, if a is the configuration of Fig. 2, all elements g either leave a invariant, or give rise to the configuration translated by one step, e.g., in the x direction. If the configuration a is highly "irregular," the orbit contains N_G configurations.

Let us denote by H_a the subgroup of G consisting of the group elements that leave invariant the configuration a:

$$H_a=\{h:\ ha=\pm a,\ h\in G\} \ . \tag{2.14}$$

Hence $g_1a=\pm g_2a$ if and only if $g_2^{-1}g_1\in H_a$. This implies that g_1 and g_2 belong to the same left coset of H_a; furthermore, denoting by N_{H_a} the number of elements of H_a, we have $N_a=N_G/N_{H_a}$. Choosing a representative element l_i $(i=1,2,\ldots,N_a)$ in each left coset lH_a, the orbit O_a is the set $\{l_i,a:\ i=1,2,\ldots,N_a\}$. Varying a over a set I of nonequivalent configurations, we obtain the set

FIG. 1. Generic spin configurations a and $b=ga$ (see text).

FIG. 2. Highly symmetric configurations a and $b=ga$ (see text).

of *all* possible configurations of spin-up electrons $\{l_i,a: a\in I,\ i=1,2,\ldots,N_a\}$. In other words, choosing $a\in I$ we fix the "form" of the configuration, choosing l_i we fix the appropriate "translation."

In the same way, all the configurations of spin-down electrons can be written as $\{\bar{l}_i\bar{a}:\ \bar{a}\in\bar{I},\ i=1,2,\ldots,N_{\bar{a}}\}$. Combining the results for both types of spin, we obtain the set of configurations $\{|la,\bar{l}\bar{a}\rangle\}$, where $a\in I$, $\bar{a}\in\bar{I}$, and $l,\bar{l}$ are chosen in the left cosets of H_a, $H_{\bar{a}}$, respectively. The concepts of equivalence and orbit can be extended to these arbitrary configurations: the states $|\phi,\bar{\phi}\rangle$ and $|g\phi,g\bar{\phi}\rangle$ are said to be *equivalent;* indeed they are physically equivalent. The *orbit* of $|\phi,\bar{\phi}\rangle$ is the set $\{|g\phi,g\bar{\phi}\rangle;\ g\in G\}$. The existence of the equivalence relation implies that the orbits are coincident or disjoint. In a given orbit we can choose an element of the type $|a,\bar{l}\bar{a}\rangle$, with $a\in I$, $\bar{a}\in\bar{I}$, and $\bar{l}$ in the left coset of $H_{\bar{a}}$, and generate all other elements of the orbits by applying the group operations $g\in G$. Therefore an orbit is characterized by three labels $a,\bar{a},\bar{l}$, and will be denoted by $O_{a,\bar{a},\bar{l}}$.

Two orbits with different values of $(a,\bar{a})$ are distinct. However, it can happen that two configurations $|a,\bar{l}_1\bar{a}\rangle$ and $|a,\bar{l}_2\bar{a}\rangle$ generate the same orbit. Therefore it is important to examine in more detail the condition of equivalence of the configurations $|a,\bar{l}_1\bar{a}\rangle$ and $|a,\bar{l}_2\bar{a}\rangle$:

$$g|a,\bar{l}_1\bar{a}\rangle=\pm|a,\bar{l}_2\bar{a}\rangle\ . \tag{2.15}$$

This equation splits into two relations,

$$g|a\rangle=\pm|a\rangle=(-1)^{S(g,a)}|a\rangle\ , \tag{2.16}$$

$$g\bar{l}_1|\bar{a}\rangle=\pm\bar{l}_2|\bar{a}\rangle\ . \tag{2.17}$$

From Eq. (2.16) it follows that $g=h_a\in H_a$. From (2.17) it follows that $\bar{l}_2^{-1}g\bar{l}_1=h_{\bar{a}}\in H_{\bar{a}}$. Hence we obtain the relation

$$h_a\bar{l}_1=\bar{l}_2h_{\bar{a}}\ . \tag{2.18}$$

This condition implies that the orbits $O_{a,\bar{a},\bar{l}_1}$ and $O_{a,\bar{a},l_2}$ coincide.

Let us now consider the linear space $L_{a,\bar{a}}(\bar{l})$ generated by the orbit $O_{a,\bar{a},\bar{l}}$:

$$\begin{aligned}L_{a,\bar{a}}(\bar{l})&=\mathrm{Span}\{g|a,\bar{l}\bar{a}\rangle,\ \ g\in G\}\\&=\mathrm{Span}\{l_i|a,\bar{l}\bar{a}\rangle,\ \ i=1,2,\ldots,N_a\}\ .\end{aligned} \tag{2.19}$$

By Eq. (2.6) we can also write

$$L_{a,\bar{a}}(\bar{l})=\mathrm{Span}\{v^j_{\mu m}|a,\bar{l}\bar{a}\rangle\}\ . \tag{2.20}$$

The dimension of the eigenvalue problem is greatly reduced by assuming the vectors $v^j_{\mu m}|a,\bar{l}\bar{a}\rangle$ as basis vectors, with j and m fixed. The group element $\bar{l}$ modifies the relative position of the configurations $a,\bar{a}$ and the operator $v^j_{\mu m}$ gives rise to a vector of the standard basis with respect to the space group. The vectors $v^j_{\mu m}|a,\bar{l}\bar{a}\rangle$ and $v^{j'}_{\mu' m'}|a,\bar{l}\bar{a}\rangle$ are orthogonal if $j\neq j'$ or $m\neq m'$; however, the vectors $v^j_{\mu m}|a,\bar{l}_1\bar{a}\rangle$ and $v^j_{\mu' m}|a,\bar{l}_2\bar{a}\rangle$ are not orthogonal if condition (2.18) is verified. Indeed we have, using Eqs. (2.8) and (2.3),

$$\begin{aligned}\langle a,\bar{l}_2\bar{a}|v^{j\dagger}_{\mu' m}v^j_{\mu m}|a,\bar{l}_1a\rangle&=\sqrt{N_G/d_j}\,\langle a,\bar{l}_2\bar{a}|v^j_{\mu\mu'}|a,\bar{l}_1\bar{a}\rangle\\&=\sum_g\overline{D^j_{\mu'\mu}(g)}\langle a,\bar{l}_2\bar{a}|ga,g\bar{l}_1\bar{a}\rangle\ .\end{aligned} \tag{2.21}$$

The scalar product inside the sum vanishes unless $g=h_a\in H_a$ and $\bar{l}_2|\bar{a}\rangle=\pm h_a\bar{l}_1|\bar{a}\rangle$, i.e., unless Eq. (2.18) holds. In the last case we can write

$$|ga,g\bar{l}_1\bar{a}\rangle=(-1)^{S(h_a,a)+S(h_{\bar{a}},\bar{a})}|a,\bar{l}_2\bar{a}\rangle\ , \tag{2.22}$$

and Eq. (2.21) becomes

$$\begin{aligned}&\langle a,\bar{l}_2\bar{a}|v^{j\dagger}_{\mu' m}v^j_{\mu m}|a,\bar{l}_1\bar{a}\rangle\\&\qquad=\sum_{h_a}\overline{D^j_{\mu'\mu}(h_a)}(-1)^{S(h_a,a)+S(h_{\bar{a}},\bar{a})}\ ,\end{aligned} \tag{2.23}$$

where the sum $\sum_{h_a}$ is restricted to the $h_a\in H_a$ such that $\bar{l}_2^{-1}h_a\bar{l}_1\in H_{\bar{a}}$. Taking into account the preceding discussion [see in particular Eq. (2.19)] an arbitrary state vector describing the system can be written as

$$|\psi\rangle=\sum_{a,\bar{a},l,\bar{l}}c_{a\bar{a}\bar{l}l}|a,\bar{l}\bar{a}\rangle\ , \tag{2.24}$$

where $a,\bar{a}$ and $\bar{l}$ determine the orbit $O_{a,\bar{a},\bar{l}}$ and l runs over N_a representative elements chosen in the left cosets of H_a.

Let us apply to the state $|\psi\rangle$ the projection operator P^j_m; we obtain the basis vector

$$\begin{aligned}|\psi^j_m\rangle&=P^j_m|\psi\rangle\\&=\sum_{a,\bar{a},l,\bar{l}}c_{a\bar{a}\bar{l}l}\sum_\mu\sqrt{d_j/N_G}\,D^j_{m\mu}(l)v^j_{\mu m}|a,\bar{l}\bar{a}\rangle\ .\end{aligned} \tag{2.25}$$

Finally, introducing the coefficient:

$$u^{(\mu)}_{a,\bar{a},\bar{l}}=\sqrt{d_j/N_G}\sum_l c_{a\bar{a}\bar{l}l}D^j_{m\mu}(l)\ , \tag{2.26}$$

we can write

$$|\psi^j_m\rangle=\sum_{a,\bar{a},\bar{l},\mu}u^{(\mu)}_{a,\bar{a},\bar{l}}v^j_{\mu m}|a,\bar{l}\bar{a}\rangle\ . \tag{2.27}$$

The vectors $|\psi^j_m\rangle$ constitute a suitable basis for studying the eigenvalue problem for the Hamiltonian (1.1) in a given invariant subspace. Let us write the "kinetic-energy" operator T as $K+\bar{K}$, where K refers to spin-up

electrons and $\bar{K}$ to spin-down electrons. Since the group operations commute with K, we have

$$K|a\rangle = \sum_i k_i l_i |b_i\rangle ,$$

where the configurations $l_i|b_i\rangle$ are obtained from $|a\rangle$ by letting one electron make a shift between nearest-neighbor sites.

$$K|\psi_m^j\rangle = \sum_{a,\bar{a},\bar{l},\mu} u_{a,\bar{a},\bar{l}}^{(\mu)} v_{\mu m}^j K|a,\bar{l}\bar{a}\rangle$$
$$= \sum_{a,\bar{a},\bar{l},\mu} u_{a,\bar{a},\bar{l}}^{(\mu)} v_{\mu m}^j \sum_i k_i |l_i b_i,\bar{l}\bar{a}\rangle . \quad (2.28)$$

Setting

$$|\psi_{a\bar{a}}^{i\mu}\rangle = \sum_{\bar{l}} u_{a,\bar{a},\bar{l}}^{(\mu)} |b_i, l_i^{-1}\bar{l}\bar{a}\rangle \quad (2.29)$$

and using Eq. (2.5), we can write

$$K|\psi_m^j\rangle = \sum_{a,\bar{a},i,\mu,\nu} D_{\mu\nu}^j(l_i) v_{\nu m}^j |\psi_{a\bar{a}}^{i\mu}\rangle . \quad (2.30)$$

From (2.29) we see that

$$|\psi_{a\bar{a}}^{i\mu}\rangle = \sum_{\hat{l}} d(\hat{l}) |b_i, \hat{l}\bar{a}\rangle , \quad (2.31)$$

where the elements $\hat{l}$ are chosen in the left cosets of $H_{\bar{a}}$; the coefficients $d(\hat{l})$ are given by

$$d(\hat{l}) = \sum_{\bar{l}} \langle b_i, \hat{l}\bar{a}|b_i, l_i^{-1}\bar{l}\bar{a}\rangle u_{a,\bar{a},\bar{l}}^{(\mu)}$$
$$= \sum_{\bar{l}} \langle l_i \hat{l}\bar{a}|\bar{l}\bar{a}\rangle u_{a,\bar{a},\bar{l}}^{(\mu)}$$
$$= (-1)^{S(l_*^{-1} l_i \hat{l}, \bar{a})} u_{a,\bar{a},\bar{l}_*}^{(\mu)} , \quad (2.32)$$

where $\bar{l}_*$ denotes the representative element chosen in the left coset of $H_{\bar{a}}$ that contains $l_i\hat{l}$.

Formulas (2.30)–(2.32) allow one to compute $K|\psi_m^j\rangle$. We can proceed in the same way in order to obtain the expansion of $\bar{K}|\psi_m^j\rangle$ in our basis:

$$\bar{K}|\psi_m^j\rangle = \sum_{a,\bar{a},\bar{l},\mu} u_{a,\bar{a},\bar{l}}^{(\mu)} v_{\mu m}^j |a,\bar{K}\,\bar{l}\bar{a}\rangle$$
$$= \sum_{a,\mu} v_{\mu m}^j \sum_{\bar{a}_1,\bar{l}_1} c(\bar{l}_1)|a,\bar{l}_1\bar{a}_1\rangle , \quad (2.33)$$

where the Fourier coefficients $c(\bar{l}_1)$ can be easily computed since the spin-up configuration a is unaffected by $\bar{K}$:

$$\bar{K}|\bar{a}\rangle = \sum_i \bar{k}_i l_i |b_i\rangle ,$$
$$c(\bar{l}_1) = \sum_{\bar{a},\bar{l}} u_{a,\bar{a},\bar{l}}^{(\mu)} \langle \bar{l}_1\, \bar{K}\bar{a}_1|\bar{l}\bar{a}\rangle$$
$$= \sum_{\bar{a},\bar{l}} \sum_i u_{a,\bar{a},\bar{l}}^{(\mu)} \bar{k}_i \langle \bar{l}_1 \bar{l}_i \bar{b}_i|\bar{l}\bar{a}\rangle . \quad (2.34)$$

The configurations $\bar{l}_i|\bar{b}_i\rangle$ are obtained from $\bar{a}_1$ by shifting a spin-down electron between nearest-neighbor sites. Only the term with $\bar{a}=\bar{b}_i$ contributes to the sum, and $\bar{l}$ must be equal to the representative element $\bar{l}_*$ chosen in the left coset of $H_{\bar{b}_i}$ containing $\bar{l}_1\bar{l}_i$. Therefore

$$c(\bar{l}_1) = \sum_i \bar{k}_i u_{a,\bar{b}_i,\bar{l}_*}^{(\mu)} (-1)^{S(\bar{l}_*^{-1}\bar{l}_1\bar{l}_i,\bar{b}_i)} . \quad (2.35)$$

The potential energy operator V is diagonal:

$$V v_{\mu m}^j |a,\bar{l}\bar{a}\rangle = U n_D(a,\bar{a},\bar{l}) v_{\mu m}^j |a,\bar{l}\bar{a}\rangle , \quad (2.36)$$

where $n_D(a,\bar{a},\bar{l})$ denotes the number of doubly occupied sites in the configuration $|a,\bar{l}\bar{a}\rangle$.

In conclusion, formula (2.30)–(2.36) provide the matrix elements of the Hubbard Hamiltonian in the basis $v_{\mu m}^j|a,\bar{l}\bar{a}\rangle$.

The space group of the Hubbard Hamiltonian, in the case of a square $n\times n$ lattice with periodic boundary conditions, is generated by five operations (see Ref. 28):

t_x: translation in the x direction by one lattice site. ($t_x^n = e$.)

t_y: translation in the y direction by one lattice site. ($t_y^n = e$.)

s_z: reflection $x' = -x$.

s_y: reflection $y' = -y$.

q: reflection with respect to the main diagonal, i.e., interchange of the x and y axis.

The number N_G of elements of G is quite large. For a 4×4 lattice $N_G = 128$. The unitary irreducible representations D^j of G can be easily found by standard methods. A short mathematical derivation is contained in the Appendix. For a square $n\times n$ lattice, a representation D^j can be labeled by five indexes k_1, k_2, b_1, b_2, c:

TABLE I. Irreducible representations in the case of the 4×4 lattice.

	k_1	k_2	b_1	b_2	c	Dimension
1	0	0	1	1	1	1
2	0	0	1	1	−1	1
3	0	0	−1	−1	1	1
4	0	0	−1	−1	−1	1
5	π	π	1	1	1	1
6	π	π	1	1	−1	1
7	π	π	−1	−1	1	1
8	π	π	−1	−1	−1	1
9	0	0	1	−1	0	2
10	π	π	1	−1	0	2
11	π	0	1	1	0	2
12	π	0	1	−1	0	2
13	π	0	−1	1	0	2
14	π	0	−1	−1	0	2
15	$\frac{\pi}{2}$	0	0	1	0	4
16	$\frac{\pi}{2}$	0	0	−1	0	4
17	$\frac{\pi}{2}$	$\frac{\pi}{2}$	0	0	1	4
18	$\frac{\pi}{2}$	$\frac{\pi}{2}$	0	0	−1	4
19	π	$\frac{\pi}{2}$	1	0	0	4
20	π	$\frac{\pi}{2}$	−1	0	0	4

$D^j=\gamma^{k_1,k_2}_{b_1,b_2,c}$. The indexes k_i $(i=1,2)$ represent momenta, since the eigenvalues of $D^j(t_x)$, $D^j(t_y)$ are respectively $e^{\pm ik_1}$, $e^{\pm ik_2}$, where $k_i=(2\pi/n)p_i$, $-\pi<k_i<\pi$, p_i integer. The numbers $b_1=\pm1$, $b_2=\pm1$, $c=\pm1$ refer to the parity under the operations s_x,s_y,q, but label different representations only for particular values of the momenta (see the Appendix). For instance the so-called "d-wave" symmetry corresponds to $k_1=k_2=0$, $s_x=s_y=1$, $q=-1$. In the case of the 4×4 lattice, there are 20 irreducible representations (see Table I).

III. RESULTS

In this section, we discuss the physical contents of the numerical data which have been obtained in the Hubbard model on a 4×4 cluster for several values of the coupling U in the case of half filling, one and two holes.

A. Ground-state symmetries

At half filling (i.e., eight spin-up electrons and eight spin-down electrons) the ground state is a nondegenerate singlet in agreement with a theorem by Lieb.[32] More precisely, the ground state is totally symmetric both with respect to the SU(2) spin group and the space group G. We also notice that, exactly at half filling, the Hubbard Hamiltonian on a bipartite lattice has an additional symmetry, known as charge conjugation, which corresponds to the unitary transformation

$$c_{i,\sigma}\rightarrow\epsilon_i c^\dagger_{i,\sigma} \tag{3.1}$$

where σ is the spin index and ϵ_i is equal to 1 on one sublattice and -1 on the other. The ground state is invariant under this symmetry and interesting consequences on the correlation functions follow. For instance, the one-particle density matrix

$$\rho(i,j)\equiv\langle c^\dagger_{i,\sigma}c_{j,\sigma}\rangle \tag{3.2}$$

vanishes whenever the two indices (i,j) belong to the same sublattice and $i\neq j$. In momentum space this gives rise to a symmetry property of the momentum distribution:

$$n(\mathbf{Q}-\mathbf{k})=1-n(\mathbf{k}) \tag{3.3}$$

where $\mathbf{Q}\equiv(\pi,\pi)$ is the nesting wave vector and

$$n(\mathbf{k})\equiv\langle c^\dagger_{\mathbf{k},\sigma}c_{\mathbf{k},\sigma}\rangle\ . \tag{3.4}$$

As a consequence, the momentum distribution at half filling is always characterized by the value $\frac{1}{2}$ on the Fermi surface of the noninteracting system, because the equality $\mathbf{k}=\mathbf{Q}-\mathbf{k}$ is satisfied modulo a reciprocal lattice vector.

The analysis of the symmetries of the ground state is more instructive in the doped system where no exact analytical statement is available. The one-hole ground state (seven spin-up electrons and eight spin-down electrons) always belongs to the minimum spin sector $(S=\frac{1}{2})$ up to very large U where the ferromagnetic state takes over, in agreement with Nagaoka theorem.[33] We explicitly checked that the total spin is $S=\frac{1}{2}$ in all the cases we have examined, i.e., for $U\leq60$. This result does not contradict previous diagonalization of the t-J model on the same cluster[22] which identified the Nagaoka transition at $J\sim0.075$ corresponding to $U=4/J\sim53$, since the correspondence between the two models holds only asymptotically at large U. As far as the space symmetries discussed in Sec. II, we have found that the ground state has total momentum belonging to the Fermi surface of the noninteracting $(U=0)$ system. This feature is preserved also at strong coupling (up to $U=60$) where the effects of the interaction are relevant and, again, agrees with previous results in the t-J model.[22] In a 4×4 lattice with periodic boundary conditions, an additional space symmetry[22] is responsible for the exact degeneracy of the lowest state belonging to two irreducible representations of G: a two-dimensional representation $\gamma^{\pi,0}_{-1,1,0}$ (see the Appendix) with total momenta $\mathbf{K}=(0,\pi)$ and $\mathbf{K}=(\pi,0)$, and a four-dimensional representation $\gamma^{\pi/2,\pi/2}_{0,0,1}$ with momenta $\mathbf{K}=(\pm\pi/2,\pm\pi/2)$. This degeneracy will be split in larger lattices and the ground state in the thermodynamic limit is believed[12] to have momenta $\mathbf{K}=(\pm\pi/2,\pm\pi/2)$.

The two-hole ground state is always a spin singlet which smoothly connects to the $J=0$ limit of the t-J model ground state. However, at $U\sim3$, a level crossing occurs between states of different space symmetry. At weak coupling, the ground state belongs to the representation $\gamma^{\pi/2,\pi/2}_{0,0,1}$ with total momenta $\mathbf{K}=(\pm\pi/2,\pm\pi/2)$ and is degenerate with the doublet of states in the representation $\gamma^{\pi,\pi}_{1,-1,0}$ of momentum $\mathbf{K}=(\pi,\pi)$ (and p rotational symmetry) because of the previously discussed additional space symmetry of the 4×4 lattice. At strong coupling, instead, the ground state belongs to the representation $\gamma^{0,0}_{1,1,-1}$ with zero total momentum and d rotational symmetry, which is degenerate with the pair of states belonging to the representation $\gamma^{\pi,0}_{1,1,0}$.

Let us now turn to the physical contents of these states, which will be extracted by analyzing the relevant correlation functions. The results of our analysis do not depend substantially on the particular choice of states in ground-state manifold.

B. Magnetic properties

The Hubbard model is generally believed to show antiferromagnetic long-range order at half filling. This picture is also consistent with the data of Fig. 3 showing the U dependence of the height of the peak in the magnetic structure factor $\mathbf{S}(\mathbf{k})$

$$S(\mathbf{k})=\frac{1}{N_s}\sum_{\mathrm{i,j}}e^{i\mathbf{k}\cdot(\mathrm{i}-\mathrm{j})}\langle S^z_{\mathrm{i}}S^z_{\mathrm{j}}\rangle\ , \tag{3.5}$$

which occurs at $\mathbf{k}=(\pi,\pi)$. The z component of the spin operators in Eq. (3.5) is defined by

$$S^z_{\mathrm{i}}\equiv(n_{\mathrm{i},\uparrow}-n_{\mathrm{i},\downarrow}) \tag{3.6}$$

in terms of the occupation numbers, and N_s is the number of sites in the lattice. This plot shows a monotonic increase with increasing U which is in striking contrast

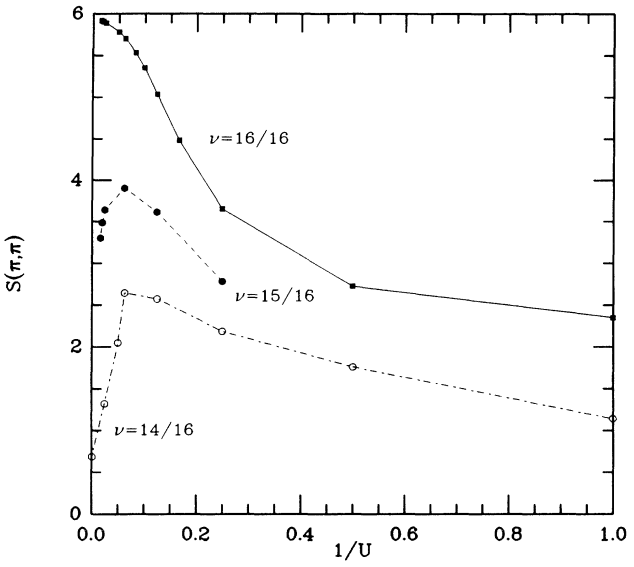

FIG. 3. Magnetic structure factor $S(\pi,\pi)$ as a function of inverse coupling for three different fillings.

with the behavior of $S(\pi,\pi)$ in the doped system. In fact the same figure also shows the structure factor in the one- and two-hole case. Two remarkable features of these plots must be stressed: (i) an overall depletion of $S(\pi,\pi)$ with increasing doping at fixed U and (ii) the presence of an optimal U for the creation of antiferromagnetic ordering in the doped system.

For both fillings ($\nu=\frac{15}{16}$ and $\frac{14}{16}$) this optimal coupling occurs at $U\sim 16$ but this critical value is most likely related to the small size of the lattice and probably tends to infinity in the thermodynamic limit. However, the frustrating effect of doping is clearly seen in Fig. 3.

Figure 4 shows a real-space picture of the spin-spin correlations at half filling for three different values of U. The data are plotted along the particular closed path in

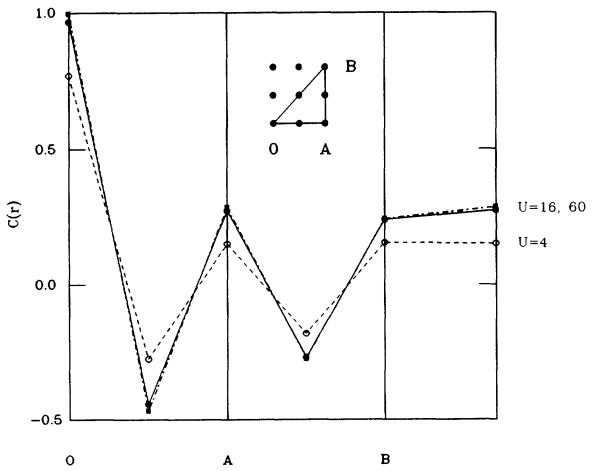

FIG. 4. Real-space picture of the spin-spin correlation function for the half-filled Hubbard model at three values of U.

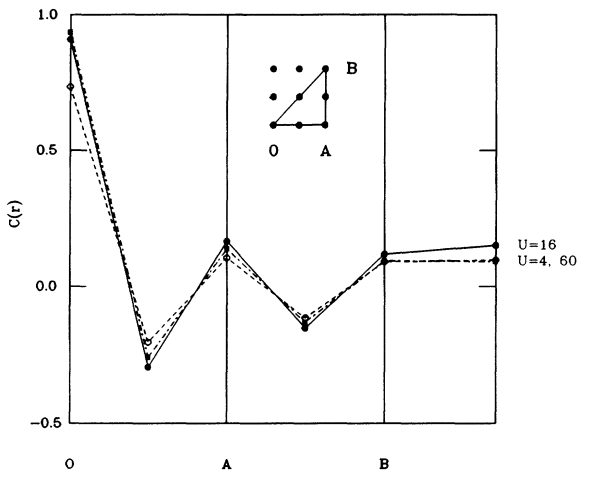

FIG. 5. As in Fig. 3 for one hole.

the 4×4 lattice shown in the inset. This kind of plot gives clear evidence of the presence of antiferromagnetic correlations in the half-filled Hubbard model. Antiferromagnetism is also shown to saturate at about $U\sim 16$, where the staggered magnetization closely approaches the Heisenberg value.[34]

The picture is quite different in the one-hole case of Fig. 5, where antiferromagnetic ordering is still present but is frustrated at large U. The same conclusion can be drawn for two holes, where the magnetic structure factor (3.1) is plotted along the closed path in $\mathbf{k}$ space shown in the inset of Fig. 6. Notice that the maximum always occurs at the corner of the Brillouin zone $\mathbf{Q}=(\pi,\pi)$, showing the tendency to the creation of antiferromagnetic ordering. The picture of Fig. 6 is consistent with an analogous calculation performed in the t-J model.[35]

The physical origin of the frustration effect induced by

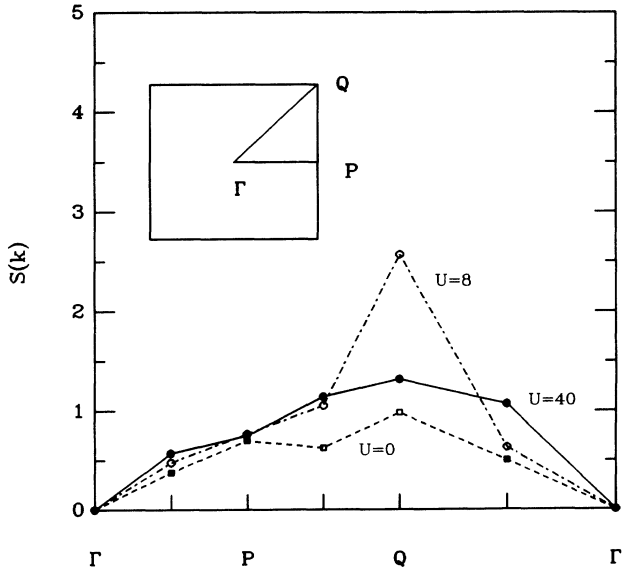

FIG. 6. Magnetic structure factor for two holes at three different couplings.

holes is widely recognized: holes gain kinetic energy by distorting the Néel spin background. However, the precise form of the resulting spin configuration is still an open problem, although incommensurate spiral ordering has received considerable theoretical support. A direct test of this conjecture in finite lattices is particularly difficult due to the competing effect of periodic boundary conditions, which favor commensurate spin configurations. As a result, only qualitative agreement can be expected between the spin correlation functions computed on a small lattice and the corresponding mean-field estimates. In fact, our data cannot be satisfactorily fitted with the form $\langle S_0^z S_{\mathbf{r}}^z \rangle \propto \cos[\pi(1-\delta)(x \pm y)]$ obtained at mean-field level,[36,37] although this expression correctly reproduces the overall depletion of $S(\pi,\pi)$ with increasing doping.

C. Spin-hole correlations

In the one-hole case, it is instructive to analyze in detail the effects of the hole on the magnetic structure previously discussed. The appropriate correlation function

$$y(\mathbf{r}) = \sum_{\mathbf{R}} \langle (1-n_{\mathbf{R},\uparrow})(1-n_{\mathbf{R},\downarrow}) S_{\mathbf{r}+\mathbf{R}}^z \rangle \tag{3.7}$$

is shown in Fig. 7 for three values of U. In order to appreciate the difference between weak and strong coupling, it is useful to analyze the predictions of two special limiting cases. Let us consider the trial wave function of total momentum $\mathbf{k}$ given by

$$|\psi^{1h}\rangle = \sqrt{2/N_s} \sum_{\mathbf{r}} e^{i\mathbf{k}\cdot\mathbf{r}} c_{\mathbf{r},\uparrow} |H\rangle \ , \tag{3.8}$$

where $|H\rangle$ is the ground state of the Hubbard model at half filling for $U \to \infty$. This is certainly an approximate wave function for arbitrary U belonging to the $S^z = -\frac{1}{2}$ subspace. Such a form is particularly convenient for calculating the spin-hole correlation function. In fact, a straightforward evaluation of (3.7) gives

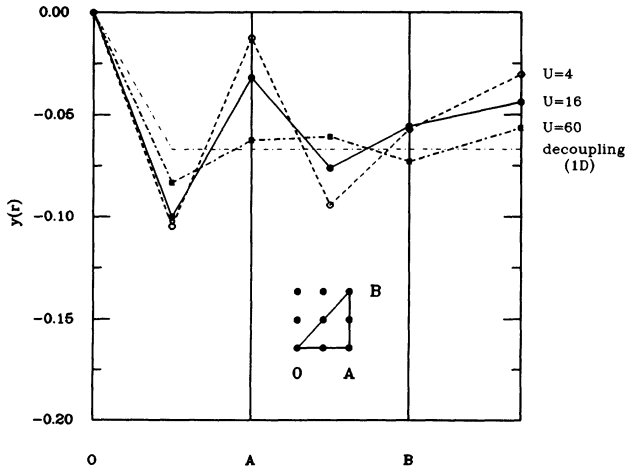

FIG. 7. Spin-hole correlation function (3.7) for one hole at three couplings. The decoupling limit is also shown.

$$y(\mathbf{r}) = \langle H | S_0^z S_{\mathbf{r}}^z | H \rangle (1-\delta_{0,\mathbf{r}}) \ . \tag{3.9}$$

Therefore, in this approximation, the spin-hole correlation function should show a marked antiferromagnetic behavior. This feature is clearly present in the numerical data of Fig. 7 at weak coupling ($U=4$) although Eq. (3.8) gives only a partial representation of the actual ground-state wave function. A physical understanding of spin-hole correlations in an antiferromagnetic environment is provided by the semiclassical analysis of Ref. 12, where it is argued that the long-range behavior of $y(\mathbf{r})$ is characterized by a power-law decay of dipolar form: $y(\mathbf{r}) \sim \mathbf{p}\cdot\mathbf{r}/r^2$, the dipolar moment $\mathbf{p}$ being a function of the coupling. This result follows from the spiral character of the spin distortion around a hole. As previously discussed, it is quite difficult to interpret our numerical data on the basis of this picture because of the sensitivity of the theoretical results to boundary conditions which inhibit incommensurate spin ordering. Moreover, the correlation function $y(\mathbf{r})$ (3.7) is not rotationally invariant in spin space and this fact introduces further uncertainty in the comparison between the numerical diagonalization, which preserves O(3) invariance, and mean-field calculations, which break this symmetry.

The magnetic environment around a hole is, instead, quite different at strong coupling ($U=60$) where the spin-hole correlation is remarkably flat. This may be considered as a signal of spin-charge decoupling. In fact, in the $U \to \infty$ 1D Hubbard model, where a spin-charge decoupling is known to occur, the spin-hole correlation function is rigorously constant. This can be explicitly checked from the known factorized form of the Lieb and Wu wave function, extensively discussed in Ref. 38 which gives the simple, exact result

$$y(\mathbf{r}) = \frac{1}{N_s - 1}(1-\delta_{0,\mathbf{r}}) \ . \tag{3.10}$$

The form (3.10) is also indicated in Fig. 7 with the label "decoupling" to stress the physical meaning of the spin-charge decoupling of this limit.

D. Hole-hole correlations

An exhaustive discussion of hole-hole correlations and their connections with the problem of hole binding in the system has been already presented in a former publication[30] and will not be repeated here. The plot of these correlations at filling $\frac{14}{16}$ (two holes) as a function of distance is shown in Ref. 30. Two key features emerge from these data: a short-range repulsion between holes and a weak attraction at longer range which develops for intermediate coupling $U \sim 16$. Here we just want to underline the close correlation between the increase of antiferromagnetic ordering of the two-hole state up to $U \sim 16$ and the corresponding presence of some sign of attraction between holes, which, instead, disappears at strong coupling. This coincidence indicates that the presence of an antiferromagnetic background might in fact help the creation of effective attraction between holes, in agreement with some theoretical studies.[8] Although finite-size effects are expected to be large in such a small lattice, we

believe that the study of hole-hole correlations gives reliable information about the presence of short-range hole attraction in the model. In fact, as it has been argued in Ref. 30, while the study of binding energy is strongly affected by finite-size corrections, such effects are less severe in hole-hole correlation functions.[39] An instructive example in which this conjecture can be verified is the 1D Hubbard model, where the exact solution is known and the binding energy can be explicitly calculated. Although no attraction between holes is present in the thermodynamic limit, finite lattice calculations give negative binding energies because of strong finite-size corrections.[40] Instead, the hole-electron correlation function computed by the Lanczos technique shows weak finite-size effects and correctly indicates the absence of binding even in small lattices.

E. Electronic structure

The analysis of the electronic structure in the Hubbard model is very important for the understanding of the effects of doping in Mott insulators. Unfortunately, the study of such properties is crucially limited by the low **k**-space resolution in finite systems. In particular, for a 4×4 cluster, only six points in the Brillouin zone are not related by the (rigid) space symmetries of the lattice. All these points lie along the path shown in the inset of Fig. 8, where the momentum distribution of the half-filled system is shown (solid line) for two values of the coupling U. At weak coupling $n(\mathbf{k})$ is remarkably free-particle-like with a marked jump across the Fermi surface even if the system is believed to be a Mott insulator. This is quite probably a finite-size effect already encountered in the numerical analysis of 1D systems.[21] An accurate analysis in the framework of the 2D Hubbard model has been performed in Ref. 41, where strong evidence in favor of a smooth momentum distribution has been obtained by numerical simulations. The interaction flattens the momentum distribution, which, in the $U\rightarrow\infty$ limit becomes a constant $n(\mathbf{k})=\frac{1}{2}$ because of the constraint of single-site occupancy. In the same figure, the momentum distribution for the eight spin-down electrons in the one-hole ground state (with $S^z=-\frac{1}{2}$) is also shown. Notice that, while for $U=4$ the difference between the two curves is small and limited to **k** points on the Fermi surface, at strong coupling the difference is large in the whole Brillouin zone, showing that the removal of a spin-up electron does significantly modify the momentum distribution of the electrons with opposite spin. This may be understood as the effect of releasing the single-site occupancy constraint enforced by the interaction at half filling.

It is also interesting to consider the momentum distribution for the seven spin-up electrons in the one-hole case (Fig. 9). The presence of a consistent depletion of charge outside the magnetic Brillouin zone suggests that the missing electron is spread in a large portion of momentum space and indicates that quasiparticles of this system acquire a more pronounced collective nature at strong coupling. In order to investigate quantitatively the character of the quasiparticles, we have plotted in Fig. 10 the quasiparticle weight Z as a function of the interaction parameter U:

$$Z=|\langle\psi^{1h}(\mathbf{k})|c_{\mathbf{k},\uparrow}|\psi^{0h}\rangle|^2\ , \tag{3.11}$$

where $|\psi^{1h}(\mathbf{k})\rangle$ is the one-hole ground state with momentum **k** and $|\psi^{0h}\rangle$ is the half-filled ground state, which has zero momentum. Charge conjugation symmetry forces Z to be always smaller than $\frac{1}{2}$ even in weak coupling.[42] Fig-

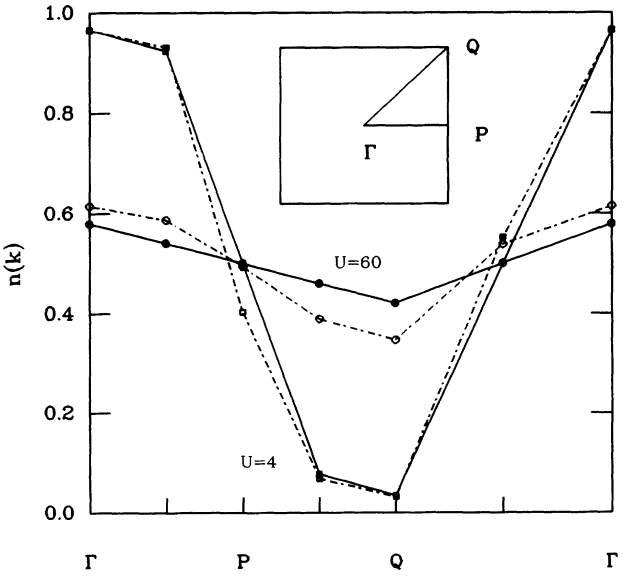

FIG. 8. Momentum distribution for the half-filled Hubbard model (solid lines) and for the (eight) spin-up electrons in the one-hole case (dashed line). The results for two couplings are shown.

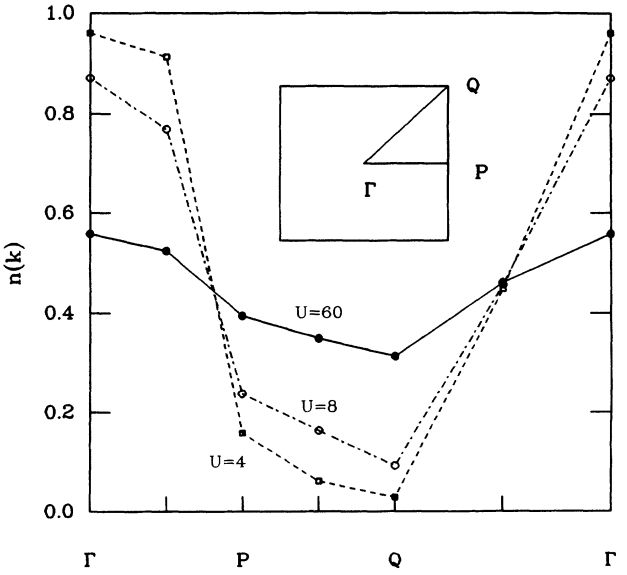

FIG. 9. Momentum distribution for the seven spin-down electrons at filling $\nu=\frac{15}{16}$ (one hole) and three different couplings.

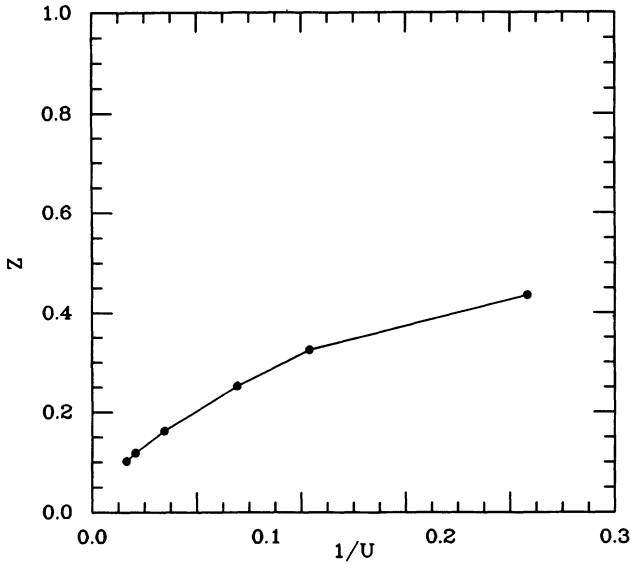

FIG. 10. Quasiparticle weight Z [Eq. (3.11)] as a function of inverse coupling.

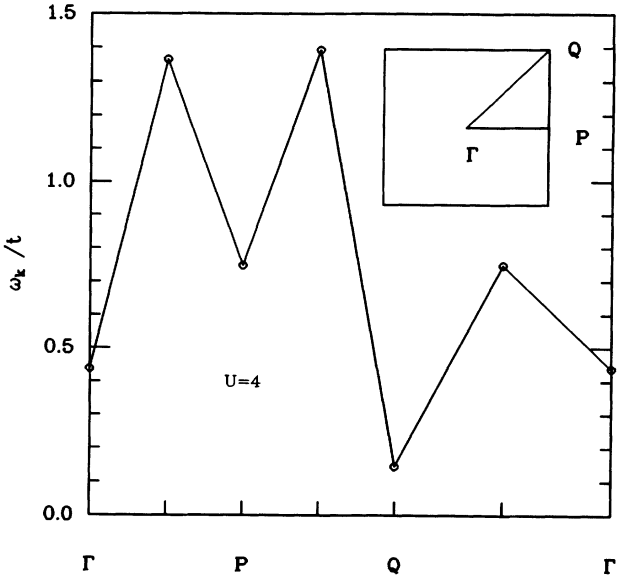

FIG. 11. Energy spectrum for triplet excitations (referred to the ground state) at half filling and $U=4$ as a function of the total momentum.

ure 10 shows the remarkable reduction in Z due to interaction, which extrapolates to a small value, possibly to zero, in the thermodynamic limit. A similar behavior has been found for Z as a function of J/t for the t-J model on a 4×4 lattice.[43] A proper finite-size scaling of the quasiparticle weight, necessarily by simulation techniques, would be quite important for understanding whether the nonzero value that we find is just due to the finiteness of the cluster or persists in the thermodynamic limit.

F. Excitation spectra

Finally, we examine the spectrum of spin and charge excitations by looking for the state of lowest energy in the various symmetry subspaces.

The energy of spin excitations at half filling is obtained by use of the Lanczos technique in the subspace of total spin $S^z=1$, i.e., in the case of nine spin-up and seven spin-down electrons. This forces the total spin to be larger than 1, thereby giving rise to the triplet excitation spectrum. The energy ω_k of an excitation as a function of the total momentum $\mathbf{k}$ is shown in Fig. 11 for $U=4$. In this case, the lowest-energy state at each fixed momentum does always belong to the irreducible representations of the space symmetry group generated by applying a spin-flip operator to the $S=0$ ground state ($\gamma^{0,0}_{1,1,1}$, $\gamma^{\pi/2,0}_{0,1,0}$, $\gamma^{\pi,0}_{-1,-1,0}$, $\gamma^{\pi,\pi/2}_{1,0,0}$, $\gamma^{\pi,\pi}_{-1,-1,1}$, $\gamma^{\pi/2,\pi/2}_{0,0,1}$). This fact suggests that the elementary spin excitations of the half-filled Hubbard model are single-particle-like and do not involve a collective rearrangement of the electrons. However, the overall shape of the spectrum does not fully agree with spin-density wave calculations,[7] which predict

$$\omega_{\mathbf{k}}^{\mathrm{SDW}} \propto \sqrt{1-\gamma_{\mathbf{k}}^2}\,, \tag{3.12}$$

where $\gamma_{\mathbf{k}}=\frac{1}{2}(\cos k_x+\cos k_y)$. This is unexpected since $U=4$ belongs to the weak (or intermediate) coupling where the spin-density wave approximation is supposed to be a good representation of the model. The main differences between the observed spectrum and Eq. (3.12) are in the absence of the degeneracy of the Γ with the Q point and the existence of the two peaks at momenta $(\pi/2,0)$ and $(\pi,\pi/2)$. However, much of the discrepancy may be attributed to finite-size effects: in particular, the two peaks in Fig. 11 are also present in the noninteracting ($U=0$) system and are related to the existence of a kinetic-energy gap for excitations of those momenta in our 4×4 cluster.

The energy spectrum of one-hole states has been obtained by the Lanczos technique in each symmetry subspace at filling $\nu=\frac{15}{16}$ (i.e., seven spin-up and eight spin-down electrons) (see Fig. 12). In this case, however, the lowest-energy state at a given momentum $\mathbf{k}$ does not always belong to the same irreducible representation as the wave function (3.8) and therefore does not correspond to the position of a pole in the Green's function of the half-filled Hubbard model. In this case the charge excitation cannot be considered one-particle-like but rather represents a collective excitation involving more than one quasiparticle. This happens at the high-symmetry points Γ and Q, where we have indicated by a dot the lowest-energy attainable at that given momentum when it does not coincide with the quasiparticle energy ($\circ$). The representations corresponding to the lowest energy at momenta Γ and Q are $\gamma^{0,0}_{-1,-1,1}$ and $\gamma^{\pi,\pi}_{1,1,1}$, respectively. Again, the observed spectrum does not coincide with the expected one[7,8]

$$\omega_{\mathbf{k}}=\sqrt{\Delta_{\mathrm{SDW}}^2+16\gamma_{\mathbf{k}}^2}\,, \tag{3.13}$$

mainly because of the presence of low-energy excitations at momentum $\mathbf{Q}=(\pi,\pi)$.

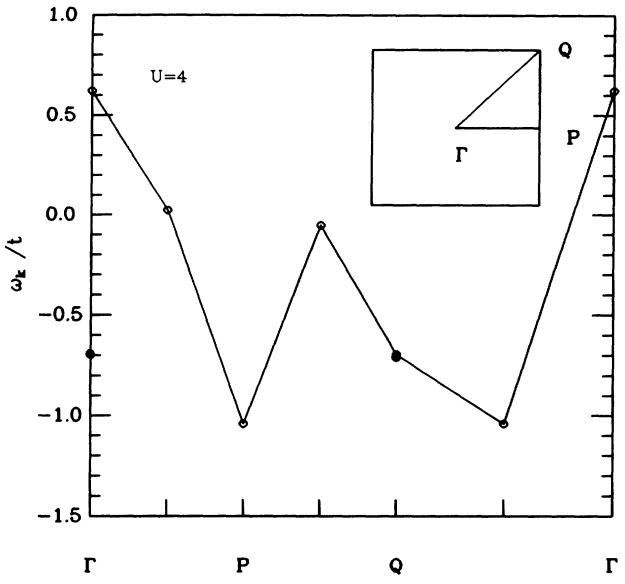

FIG. 12. Energy spectrum for one hole (referred to the half-filled ground state) at $U=4$ as a function of the total momentum.

IV. CONCLUSIONS

In this paper we have presented a survey of diagonalization results of the Hubbard model on a 4×4 cluster. In order to develop an efficient Lanczos algorithm for such a model, a careful group-theoretical analysis of the space symmetry of the system has been performed. This preliminary theoretical study has effectively reduced the dimension of the Hilbert space by two orders of magnitude. We believe that such an approach is general and might be useful in other problems where the huge dimensions of the Hilbert space do not allow a straightforward implementation of standard algorithms.

Several interesting conclusions about the physical properties of the Hubbard model can be extracted from the correlation functions previously discussed:

(1) Short-range antiferromagnetism is still present in the lattice after 10% doping, although its magnitude is considerably reduced by the presence of holes. In the doped system, interaction favors antiferromagnetism up to a critical (density-dependent) coupling $U=U_c(\rho)$. At stronger coupling a sharp decrease of antiferromagnetic ordering emerges from the numerical data.

(2) The previous results and the magnetic properties are consistent with the structure of the spin-hole correlation function, which retains antiferromagnetic correlations at weak or intermediate coupling but suggests spin-charge decoupling at larger U.

(3) Holes are shown to repel at short range for every coupling. Weak attractive correlations are seen at intermediate U and seem enhanced by the presence of local antiferromagnetism.

(4) The charge excitations acquire a more and more pronounced collective character at strong coupling, leading to a considerable reduction of the wave-function renormalization factor Z [Eq. (3.11)].

(5) Both the spin-wave spectrum and the hole spectrum present some anomalies with respect to standard theoretical expectations.

We believe that the main conclusions of this study (1–5) remain true in the thermodynamic limit and we hope that they might stimulate further Monte Carlo investigations as well as more quantitative analytical studies on the Hubbard model.

ACKNOWLEDGMENTS

This work has been supported by the Italian Ministry of University and Scientific Research and (A.P.) by Consorzio Interuniversitario di Fisica della Materia. Two of us (G.F. and F.O.) were supported in part by INFN, Sezione di Bologna. We would like to thank E. Tosatti for constant encouragement.

APPENDIX

In this appendix we study the irreducible representations D^j of the space group G of an $n\times n$ Hubbard model with periodic boundary conditions.

We recall that a subgroup T of a group G is said to be of index two if $G=\{T,sT\}$, where s is a representative taken in the left coset of T; T is necessarily an invariant subgroup. If $s^2=e$, where e is the identity, G can be written as the semidirect product $T\otimes_s\{e,s\}$ (See Ref. 44).

From the knowledge of the irreducible representations d^j of T we can easily obtain all irreducible representations of G. Since T is an invariant subgroup, for any $t\in T$, $s^{-1}ts=sts\in T$. The following representation of T:

$$\tilde{d}^{\,j}(t)=d^j(sts),\quad \forall t\in T \tag{A1}$$

is said to be *conjugate* to d. There are two different cases.

(a) $\tilde{d}$ is equivalent to d^j, i.e., $\tilde{d}^{\,j}=U^{-1}d^jU$. Then it can be proved that (see Ref. 37)

$$\Gamma=\{d^j(t),Ud^j(t),\ t\in T\}\ , \tag{A2}$$

$$\Gamma'=\{d^j(t),-Ud^j(t),\ t\in T\} \tag{A3}$$

are irreducible representations of $G=\{T,sT\}$. Clearly the element s is represented by $\pm U$.

(b) $\tilde{d}$ is not equivalent to d^j. Then it can be proved that

$$\Gamma''=\left\{\begin{bmatrix} d^j(t) & 0 \\ 0 & \tilde{d}^{\,j}(t)\end{bmatrix},\ \begin{bmatrix} 0 & \tilde{d}^{\,j}(t) \\ d^j(t) & 0\end{bmatrix},\ t\in T\right\} \tag{A4}$$

is an irreducible representation of $G=\{T,sT\}$. Furthermore *all* the irreducible representations of G can be found by formulas (A2)–(A4).

By repeated application of the semidirect product operation we can obtain the space group G. Let us denote by T_x (T_y) the subgroup of the translations in the x (y) direction. The operations t_x,t_y,s_x,s_y,q have been defined in Sec. II. We denote by H_x, H_y the subgroups

$$H_x=\{T_x,s_xT_x\}\ , \tag{A5}$$

$$H_y=\{T_y,s_yT_y\}\ . \tag{A6}$$

A different subgroup is obtained by taking the direct

product of H_x, H_y:

$$H = H_x \otimes H_y = \{ T_x T_y,\ s_x T_x T_y,\ s_y T_x T_y,\ s_x s_y T_x T_y \} . \tag{A7}$$

Finally, the space group G is obtained by taking the semidirect product of H and $\{e,q\}$, i.e.,

$$G = \{H, qH\} . \tag{A8}$$

The irreducible representations of the abelian subgroups T_x, T_y are given by

$$\{ d^{k_1}(t_x^{j_1}) = e^{ik_1 j_1},\ k_1 = \frac{2\pi}{n} p_1,\ -\pi < k_1 \le \pi,\ p_1 \text{ integer} \} , \tag{A9}$$

$$\{ d^{k_2}(t_y^{j_2}) = e^{ik_2 j_2},\ k_2 = \frac{2\pi}{n} p_2,\ -\pi < k_2 \le \pi,\ p_2 \text{ integer} \} , \tag{A10}$$

where $j_1, j_2 = 1, 2, \ldots, n-1$. Let us consider an arbitrary translation $t_x^{j_1}$, $j_1 = 1, 2, \ldots, n-1$. Since $s_x t_x^{j_1} s_x = t_x^{-j_1}$, the representation $\tilde{d}^{k}$ of T_x is given by

$$\begin{aligned} \tilde{d}^{k_1}(t_x^{j_1}) = d^{k_1}(s_x t_x^{j_1} s_x) = d^{k_1}(t_x^{-j_1}) = e^{-ik_1 j_1} \\ = d^{-k_1}(t_x^{j_1}) \\ = \overline{d^{k_1}(t_x^{j_1})} . \end{aligned} \tag{A11}$$

Therefore $\tilde{d}^{k_1}$ is equivalent (and coincident) with d^{k_1} if $k_1 = 0$ or $k_1 = \pi$ and in this case $U = 1$. The opposite happens if $0 < k_1 < \pi$. Applying formulas (A2)–(A4) we obtain the representations $\gamma_{b_1}^{k_1}$ of the group H_x, where $k_1 = 0, \pi$, $b_1 = \pm 1, 0$ (the value $b_1 = 0$ must be considered only if $0 < k_1 < \pi$):

$$k_1 = 0,\quad b_1 = 1,\quad \begin{cases} \gamma_1^0(t_x^{j_1}) = 1 \\ \gamma_1^0(s_x t_x^{j_1}) = 1 \end{cases} \tag{A12}$$

$$k_1 = 0,\quad b_1 = -1,\quad \begin{cases} \gamma_{-1}^0(t_x^{j_1}) = 1 \\ \gamma_{-1}^0(s_x t_x^{j_1}) = -1 \end{cases} \tag{A13}$$

$$k_1 = \pi,\quad b_1 = 1,\quad \begin{cases} \gamma_1^\pi(t_x^{j_1}) = e^{i\pi j_1} \\ \gamma_1^\pi(s_x t_x^{j_1}) = e^{i\pi j_1} \end{cases} \tag{A14}$$

$$k_1 = \pi,\quad b_1 = -1,\quad \begin{cases} \gamma_{-1}^\pi(t_x^{j_1}) = e^{i\pi j_1} \\ \gamma_{-1}^\pi(s_x t_x^{j_1}) = -e^{i\pi j_1} \end{cases} . \tag{A15}$$

Notice that $\gamma_b^k(s_x) = b$ for $k = 0$ or $k = \pi$. For $0 < k_1 < \pi$, $b_1 = 0$, we have

$$\begin{aligned} \gamma_0^{k_1}(t_x^{j_1}) &= \begin{bmatrix} e^{ik_1 j_1} & 0 \\ 0 & e^{-ik_1 j_1} \end{bmatrix} , \\ \gamma_0^{k_1}(s_x t_x^{j_1}) &= \begin{bmatrix} 0 & e^{-ik_1 j_1} \\ e^{ik_1 j_1} & 0 \end{bmatrix} . \end{aligned} \tag{A16}$$

The representation $\gamma_0^{k_1}$ is equivalent to the following real representation:

$$\begin{aligned} \gamma_0^{k_1 R}(t_x^{j_1}) &= \begin{bmatrix} \cos(k_1 j_1) & -\sin(k_1 j_1) \\ \sin(k_1 j_1) & \cos(k_1 j_1) \end{bmatrix} , \\ \gamma_0^{k_1 R}(s_x t_x^{j_1}) &= \begin{bmatrix} \sin(k_1 j_1) & \cos(k_1 j_1) \\ \cos(k_1 j_1) & -\sin(k_1 j_1) \end{bmatrix} . \end{aligned} \tag{A17}$$

Of course the group H_y is isomorphic to H_x and therefore the irreducible representations of H_y are equal to those of H_x. The irreducible representations of $H = H_x \otimes H_y$ are given by the direct product of $\gamma_{b_1}^{k_1}$ and $\gamma_{b_2}^{k_2}$; for any $h_x \in H_x$, $h_y \in H_y$, we have

$$\gamma_{b_1,b_2}^{k_1,k_2}(h_x h_y) = \gamma_{b_1}^{k_1}(h_x) \otimes \gamma_{b_2}^{k_2}(h_y) . \tag{A18}$$

We can now consider the space group $G = \{H, qH\}$. Since q interchanges the x and y axis, $q t_x q = t_y$, $q s_x q = s_y$. The representation of H conjugate to $\gamma_{b_1,b_2}^{k_1,k_2}$ is given by

$$\begin{aligned} \tilde{\gamma}_{b_1,b_2}^{k_1,k_2}(s_x^{\sigma_x} t_x^{j_1} s_y^{\sigma_y} t_y^{j_2}) &= \gamma_{b_1,b_2}^{k_1,k_2}(q s_x^{\sigma_x} t_x^{j_1} s_y^{\sigma_y} t_y^{j_2} q) \\ &= \gamma_{b_1,b_2}^{k_1,k_2}(s_y^{\sigma_x} t_y^{j_1} s_x^{\sigma_y} t_x^{j_2}) = \gamma_{b_1,b_2}^{k_1,k_2}(s_x^{\sigma_y} t_x^{j_2} s_y^{\sigma_x} t_y^{j_1}) \\ &= \gamma_{b_1}^{k_1}(s_x^{\sigma_y} t_x^{j_2}) \otimes \gamma_{b_2}^{k_2}(s_y^{\sigma_x} t_y^{j_1}) = \gamma_{b_1}^{k_1}(s_y^{\sigma_y} t_y^{j_2}) \otimes \gamma_{b_2}^{k_2}(s_x^{\sigma_x} t_x^{j_1}) \\ &= U^{-1} \gamma_{b_2}^{k_2}(s_x^{\sigma_x} t_x^{j_1}) \otimes \gamma_{b_1}^{k_1}(s_y^{\sigma_y} t_y^{j_2}) U . \end{aligned} \tag{A19}$$

Hence the representation conjugate to $\gamma_{b_1,b_2}^{k_1,k_2}$ is equivalent to $\gamma_{b_2,b_1}^{k_2,k_1}$. If the pairs (k_1,b_1) and (k_2,b_2) coincide, we obtain the following representations of G:

$$\gamma_{b,b,1}^{k,k} = \{ \gamma_{b,b}^{k,k}(h), U\gamma_{b,b}^{k,k}(h),\ h \in H \},\quad \gamma_{b,b,-1}^{k,k} = \{ \gamma_{b,b}^{k,k}(h), -U\gamma_{b,b}^{k,k}(h),\quad h \in H \} . \tag{A20}$$

If (k_1,b_1) and (k_2,b_2) do not coincide, $\tilde{\gamma}^{k_1,k_2}_{b_1,b_2}$ is not equivalent to $\gamma^{k_1,k_2}_{b_1,b_2}$ and we obtain the following representation:

$$\gamma^{k_1,k_2}_{b_1,b_2,0}=\left\{\begin{pmatrix}\gamma^{k_1,k_2}_{b_1,b_2}(h) & 0\\ 0 & \tilde{\gamma}^{k_1,k_2}_{b_1,b_2}(h)\end{pmatrix},\begin{pmatrix}0 & \tilde{\gamma}^{k_1,k_2}_{b_1,b_2}(h)\\ \gamma^{k_1,k_2}_{b_1,b_2}(h) & 0\end{pmatrix}\right\}, \tag{A21}$$

where $h\in H$. In the case of the 4×4 lattice ($n=4$), there are 20 representations: eight of order 1, six of order 2, and six of order 4 (see Table I).

[1]See, for instance, *Proceedings of the Adriatico Conference Strongly Correlated Electron Systems II,* edited by G. Baskaran, A. E. Ruckenstein, E. Tosatti, and Yu Lu (World Scientific, Singapore, 1991).

[2]J. E. Hirsch and S. Tang, Phys. Rev. Lett. **62**, 591 (1989); S. Sorella *et al.,* Int. J. Mod. Phys. B **3**, 1875 (1990).

[3]P. W. Anderson, Science **235**, 1196 (1987).

[4]V. J. Emery, S. A. Kivelson, and Q. Lin, Phys. Rev. Lett. **64**, 475 (1990).

[5]P. W. Anderson, Phys. Rev. Lett. **65**, 2306 (1990).

[6]J. E. Hirsch, Phys. Rev. Lett. **54**, 1317 (1985).

[7]See, for instance, E. Fawcett, Rev. Mod. Phys. **60**, 209 (1988).

[8]J. R. Schrieffer, X. G. Wen, and S. C. Zhang, Phys. Rev. B **39**, 11 663 (1989).

[9]N. E. Bikers, D. J. Scalapino, and S. R. White, Phys. Rev. Lett. **62**, 961 (1989).

[10]M. Fabrizio, A. Parola, and E. Tosatti, Phys. Rev. B **44**, 1033 (1991).

[11]C. L. Kane, P. A. Lee, and N. Read, Phys. Rev. B **39**, 6880 (1989).

[12]B. I. Shraiman and E. D. Siggia, Phys. Rev. B **42**, 2485 (1990).

[13]S. A. Trugman, Phys. Rev. B **41**, 892 (1990).

[14]H. J. Schulz, Phys. Rev. Lett. **64**, 1145 (1990).

[15]X. G. Wen, F. Wilczek, and A. Zee, Phys. Rev. B **39**, 11 413 (1989).

[16]G. Kotliar and A. R. Ruckenstein, Phys. Rev. Lett. **57**, 1362 (1986).

[17]D. P. Arovas and A. Auerbach, Phys. Rev. B **38**, 316 (1988).

[18]L. Lilly, A. Muramatsu, and W. Hanke, Phys. Rev. Lett. **65**, 1379 (1990).

[19]I. Affleck and J. B. Marston, Phys. Rev. B **39**, 11 538 (1989).

[20]R. B. Laughlin, Science **242**, 525 (1988).

[21]S. Sorella *et al.,* Europhys. Lett. **8**, 663 (1989).

[22]J. Bonca, P. Prelovsek, and I. Sega, Phys. Rev. B **39**, 7074 (1989); Y. Hasegawa and D. Poilblanc, *ibid.* **40**, 9035 (1989); E. Dagotto, A. Moreo, and T. Barnes, *ibid.* **40**, 6721 (1989); E. Kaxiras, and E. Manousakis, *ibid.* **38**, 866 (1988); W. Stephan and P. Horsch, Phys. Rev. Lett. **66**, 2258 (1991).

[23]E. Dagotto, A. Moreo, R. Joynt, S. Bacci, and E. Gagliano, Phys. Rev. B **41**, 2585 (1990).

[24]K. von Szczepanski, P. Horsch, W. Stephan, and M. Ziegler, Phys. Rev. B **41**, 2017 (1990).

[25]S. Sorella and A. Parola, J. Phys. Condens. Matter **4**, 3589 (1992).

[26]A. Moreo, D. Scalapino, and E. Dagotto (unpublished).

[27]A. Parola *et al.,* Int. J. Mod. Phys. B **3**, 1865 (1989); A. Parola *et al.,* Phys. Rev. B **43**, 6190 (1991).

[28]G. Fano, F. Ortolani, and F. Semeria, Int. J. Mod. Phys. B **3**, 1845 (1989).

[29]C. N. Yang, Phys. Rev. Lett. **63**, 2144 (1989); S. C. Zhang, *ibid.* **65**, 120 (1990); E. Ercolessi, G. Morandi, and F. Ortolani (unpublished).

[30]G. Fano, F. Ortolani, and A. Parola, Phys. Rev. B **43**, 6877 (1990).

[31]E. Dagotto, A. Moreo, F. Ortolani, J. Riera, and D. Scalapino, Phys. Rev. Lett. **67**, 1918 (1991); E. Dagotto, A. Moreo, F. Ortolani, D. Poilblanc, J. Riera, and D. Scalapino, Phys. Rev. B **45**, 10 741 (1992); E. Dagotto, A. Moreo, F. Ortolani, J. Riera, and D. Scalapino, *ibid.* **45**, 10 107 (1992).

[32]E. Lieb, Phys. Rev. Lett. **62**, 1201 (1989).

[33]Y. Nagaoka, Phys. Rev. **147**, 392 (1966).

[34]J. Reger and A. P. Young, Phys. Rev. B **37**, 5978 (1988).

[35]A. Moreo, E. Dagotto, T. Jolycoeur, and J. Riera, Phys. Rev. B **42**, 6283 (1990).

[36]H. J. Schulz, Phys. Rev. Lett. **65**, 2462 (1990).

[37]E. Arrigoni, and G. C. Strinati, Phys. Rev. B **44**, 7455 (1991).

[38]M. Ogata and H. Shiba, Phys. Rev. B **41**, 2326 (1990); A. Parola, and S. Sorella, Phys. Rev. Lett. **64**, 1831 (1990).

[39]S. Sorella, A. Parola, and E. Tosatti, Int. J. Mod. Phys. B **5**, 143 (1991).

[40]R. M. Fye, M. J. Martinis, and R. T. Scalettar, Phys. Rev. B **42**, 6809 (1990).

[41]S. Sorella *et al.,* Int. J. Mod. Phys. B **3**, 149 (1989).

[42]S. Sorella (private communication).

[43]E. Dagotto and J. R. Schrieffer, Phys. Rev. B **43**, 8705 (1991).

[44]L. Jansen and M. Boon, *Theory of Finite Groups: Applications in Physics* (North-Holland, Amsterdam, 1967).